Supplemental Document

Biomedical Optics EXPRESS

Label-free skin penetration analysis using time-resolved, phase-modulated stimulated Raman scattering microscopy: supplement

Terumasa Ito,[1,2,*] Risa Iguchi,[3] Fumiaki Matsuoka,[1,2] Yoji Nishi,[3] Tsuyoshi Ogihara,[3] and Kazuhiko Misawa[1,2]

[1] *Department of Applied Physics, Tokyo University of Agriculture and Technology, 2-24-16 Naka-cho, Koganei, Tokyo 184-8588, Japan*
[2] *Department of Biomedical Engineering, Tokyo University of Agriculture and Technology, 2-24-16 Naka-cho, Koganei, Tokyo 184-8588, Japan*
[3] *Matsumoto Trading Co., Ltd., 1-13-7 Nihonbashi-Muromachi, Chuo-ku, Tokyo 103-0022, Japan*
[*] *teru-ito@cc.tuat.ac.jp*

Supplement DOI: https://doi.org/10.6084/m9.figshare.16578920

Parent Article DOI: https://doi.org/10.1364/BOE.436142

Label-free skin penetration analysis using time-resolved, phase-modulated stimulated Raman scattering microscopy: supplemental document

TERUMASA ITO,[1,2,*] RISA IGUCHI,[3] FUMIAKI MATSUOKA,[1,2] YOJI NISHI, [3] TSUYOSHI OGIHARA[3] AND KAZUHIKO MISAWA[1,2]

[1] *Department of Applied Physics, Tokyo University of Agriculture and Technology, 2-24-16 Naka-cho, Koganei, Tokyo 184-8588, Japan*
[2] *Department of Biomedical Engineering, Tokyo University of Agriculture and Technology, 2-24-16 Naka-cho, Koganei, Tokyo 184-8588, Japan*
[3] *Matsumoto Trading Co.,Ltd., 1-13-7 Nihonbashi-Muromachi, Chuo-ku, Tokyo 103-0022, Japan*
**teru-ito@cc.tuat.ac.jp*

1. Sample preparation

Ectoine (ECT: Merck KGaA, Germany), lidocaine hydrochloride (LID: FUJIFILM Wako Pure Chemicals Corporation, Japan), and loxoprofen sodium salt dihydrate (LOX: FUJIFILM Wako Pure Chemicals Corporation, Japan) were used as the test substances in the penetration experiments. All test compounds were dissolved in pure water at room temperature.

We used a reconstructed human epidermis (EpiDerm 606-X, Mattek) as an *in vitro* skin tissue model. A tissue disk (20 mm in diameter) was cut from the cell culture cup, and the underlying membrane film was removed to minimize the optical scattering loss. The tissue disk was then placed on a glass slide with a cavity, as shown in Fig. 1(a). The space between the bottom layer of the tissue and the surface of the glass slide cavity was filled with the receiver solution, which was 20 μL of 1× phosphate-buffered saline. Next, 50 μL donor aqueous solution was dropped onto the superficial cornified layer within the inner hole of a steel washer (thickness: 1 mm, inner diameter: 6 mm). The corresponding applied dose (190 μL/cm^2) was considered as the infinite dose condition; the change in the concentration of the donor solution during the measurements was negligibly small. Finally, a 0.15-mm-thick coverslip was placed on top of the washer to enclose the donor solution. To prevent any possible leakage of the applied solution, the interfaces between the washer and the tissue disk and between the washer and the coverslip were sealed with silicone grease. The thickness of the skin tissue model measured by *XZ* confocal reflection imaging was typically ~50 μm. In the skin penetration measurement of the LID and the LOX, the sample slide was placed on a 0.5-mm-thick glass heater plate (TPi-SQX, TOKAI HIT) to keep the sample temperature at 32 ℃.

2. Microscope setup

The working principles of AM-SRS and PM-SRS microscopy are summarized in Fig. 1(b) and 1(c), respectively, and the optical setup of the dual SRS microscope is illustrated in Fig. S1(a)-(b). The microscope system uses a near-infrared mode-locked femtosecond laser (Vitara, Coherent: 80-MHz repetition, center wavelength: 790 nm, pulse width: < 15 fs). The laser beam is first split into two (P0 and P1+P2) via a polarizing beam splitter (PBS: PBSW-10-4/10, Sigma Koki), and the latter is further divided into P1 and P2 beams using a dichroic mirror (DM: RT785rdc, Chroma). After each beam is reflected by an end mirror, the beams are recombined and enter the microscope, where the beams are focused onto the sample using an objective lens (OBJ1: M Plan Apo NIR 100x, NA 0.50, Mitutoyo).

The P0 pulse is compressed to its Fourier-transform-limited pulse width (<15 fs) using chirped mirrors (DCMP-175, Thorlabs) and standard 4f pulse shaper optics with a transmission

grating (WP-600, Wasatch Photonics) and a spatial light modulator (LCOS-SLM, X10468-02, Hamamatsu). To obtain the fine spectral resolution by spectral-focusing (~25 cm^{-1}) and a clear temporal pump-probe separation, the two probe pulses were shaped to be temporally asymmetric picosecond pulses (rise time: 0.4 ps, fall time: 1.9 ps) [1]. Such engineered pulse shaping is realized by optimizing the group delay dispersion and higher-order dispersions. In particular, temporal asymmetry can be achieved using carefully designed bandpass filters with large odd-order dispersions (BPF1: TBP01-796/12-25×36, Semrock, and BPF2: TBP01-900/11-25×36, Semrock). Bandpass filters are also used to tune the Raman detection frequency. BPF1 defines the fixed frequency band of the P1 pulses (centered at 758 nm), and BPF2 adjusts and sweeps the P2 frequency band (centered at 782 nm to 852 nm) via filter-rotation tuning, allowing the detection frequency Ω to be tunable from 400 cm^{-1} to 1600 cm^{-1}.

In the AM-SRS mode, two picosecond pulses (P1 and P2) spatially and temporally overlap at the sample, whereas the P0 pulse is turned off. The P1 and P2 pulses, which function as so-called pump and Stokes pulses, respectively, excite the molecular vibration mode. To detect the SRS signal, the P2 (the Stokes) beam modulated at 1 MHz by an AM electro-optic modulator (EOM2: EO-AM-NR-C1, Thorlabs) was used as an AM probe, and the other P1 beam (the pump) was used as a strong local oscillator (LO). In fact, these excitation and detection processes occur simultaneously, resulting in energy transfer from the pump pulse to the Stokes pulse. After passing through the sample, the transmission beams are collected by another objective lens through a high numerical aperture (OBJ2: M PLAN APO 100x, NA 0.70, Mitutoyo). The AM Stokes beam is blocked by a bandpass filter (FF01-760/12-25, Semrock), and the stimulated Raman loss signal on the LO pump beam is detected by a photodiode (PD1: PDA36A, Thorlabs). To avoid any possible back-reflection to the mode-locked laser, an optical isolator with a Faraday rotator (ISO: EURYS, Electro-Optics Technology) is used in the pulse-shaping optics unit.

In the PM-SRS mode, a femtosecond pulse (P0) and two picosecond pulses (P1 and P2) were used to separate the excitation and detection processes in the time domain. The P0 pulse was used as an impulsive excitation pulse (functioning as a degenerated pump/Stokes pulse), by which all Raman vibrational modes within the laser bandwidth (up to 1500 cm^{-1}) were excited simultaneously. P1 and P2, both of which are equally delayed with respect to the pump pulse (by more than 0.5 ps), were used as probe pulses to selectively detect the long-lived vibrational mode. The relative temporal delay between P0 and the two probe pulses was adjusted by the *Z*-position of the end mirror on the P0 arm. The P1 pulse was used as the PM probe pulse, whereas the P2 pulse was used as the LO probe pulse. Phase-sensitive heterodyne detection was performed by applying a 2π sawtooth phase modulation at 100 kHz onto the PM probe pulse train with a PM electro-optic modulator (EOM1: EO-PM-NR-C1, Thorlabs). When the Raman frequency of the sample matches the difference in frequencies between the PM and LO probes, the input for the sawtooth phase modulation is converted to a sinusoidal SRS intensity-modulation output on the LO beam through temporal beam coupling between the two probes via Raman-induced refractive index modulation. After the sample, the pump and PM probe beams were blocked by a polarizer (GYPC-06-15SN, Sigma Koki) and a long-pass filter (ET780lp, Chroma), respectively. The remaining LO beam passing through the filter was detected using PD1. Notably, when the PM and LO probe pulses temporally overlap, nonlinear effects such as cross-phase modulation, transient absorption, as well as SRS occur. However, these are not regarded as background signals and not detected in PM-SRS. In PM heterodyne detection, nonlinear signals induced solely by the PM and LO probe pulses are always zero because phase modulation itself does not change the intensity of the pulse (i.e., the nonlinear effects are always 'ON'). This PM detection scheme can be used to extract the purely time-resolved vibrational signals generated by the excitation pulse, without being affected by SRS and other nonlinear effects induced by the probes. The average beam powers of the excitation pump/Stokes, PM probe, and LO probe beams on the sample were 35 mW, 10 mW, and <7 mM, respectively, which were optimized to achieve the best signal-to-noise ratio (S/N) while

avoiding photodamage. Based on brightfield imaging observation and monitoring of optical transmittance, we confirmed that there was no significant photodamage in any measurements.

In addition to the two SRS modes, the microscopy apparatus was designed to allow switching to the confocal reflection mode (Fig. S1(c)). We used confocal reflection microscopy to depict the layer structures and interfaces of the skin tissue. To switch to the confocal reflection mode, we inserted a quarter-wave plate and a polarizing beam splitter, which were mounted on a translational stage placed near the entrance port of the microscope. A backscattered light due to a local refractive index mismatch at the sample focal point was collected by the objective lens and detected by the PD2 (PDA36A, Thorlabs) placed behind a confocal pinhole (PH).

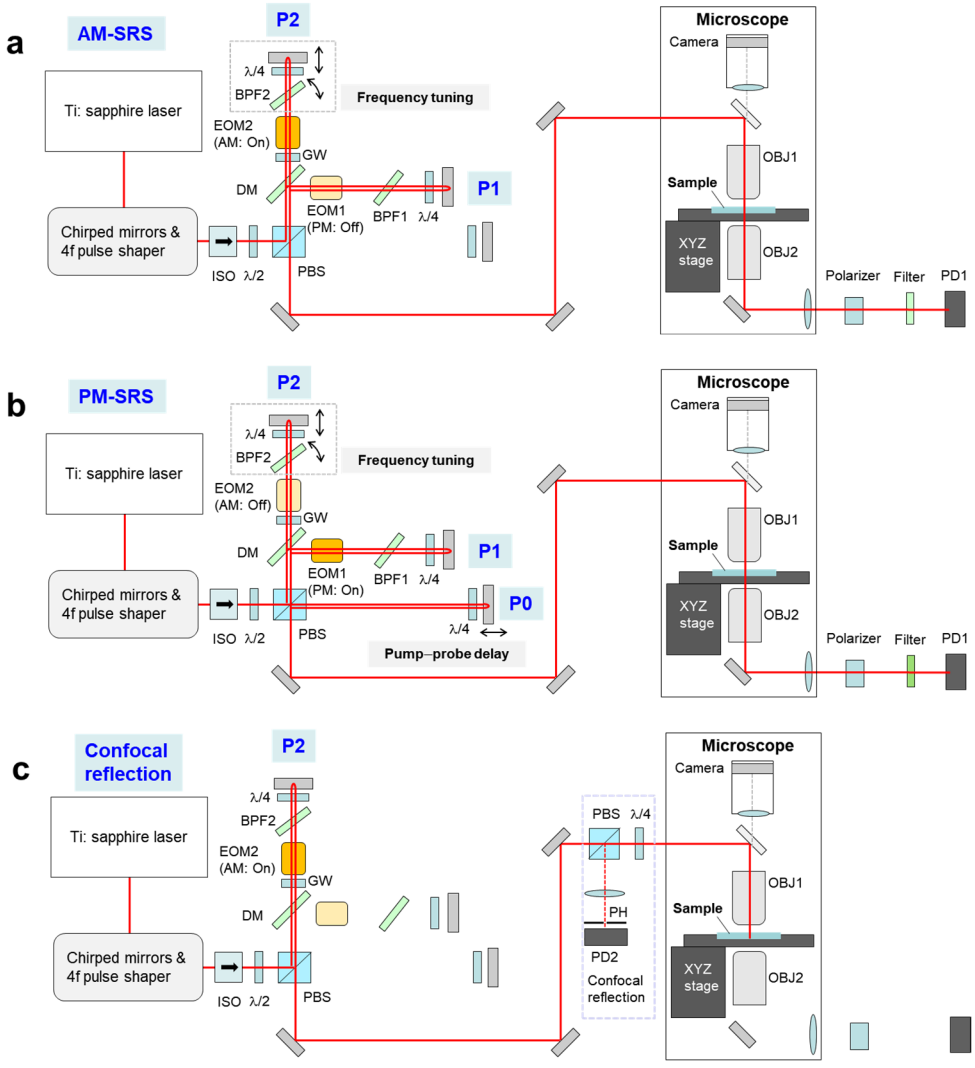

Fig. S1 Schematics of the optical setup of (a) AM-SRS, (b) PM-SRS, and (c) confocal-reflection microscopy. The double red lines represent round-trip beam paths (each probe beam passes through the EOM twice).

3. Data acquisition and signal processing

In either SRS mode, the weakly modulated signal on the LO beam was extracted using a lock-in amplifier (LIA: LI5660, NF Corporation) with a time constant of 100 μs. To acquire two-dimensional depth images, the laser beams were raster-scanned on the *XZ* plane by driving a sample stage, and the LIA output signals were acquired using a digitizer (USB 6212, National Instruments) at a sampling frequency of 10 kHz. The linear velocity of the stage scan was 1 mm/s, and the effective exposure time per single line was 200 ms. A depth image (image size: 400 × 200 pixels, field of view: 200 × 200 μm) was acquired through 200 linear scans along the *X*-direction with a line pitch of 1 μm along the *Z*-direction. The total exposure time to acquire a single image was 200 ms × 200 lines = 40 s. The total integration time of the mean SRS signals in Fig. 4(c) (-5 μm $\leq Z_r \leq$ 5 μm) was 200 ms/line × 11 lines × 8 images accumulation = 17.6 s. Raster-scanning, data acquisition, and frequency tuning were controlled using a custom graphical user interface based on LabVIEW (National Instruments), and all subsequent signal processing was performed in MATLAB (MathWorks).

When an SRS signal from a low-concentration drug (tens of mM or less) in a tissue is very weak (on the order of $\Delta I/I_{LO} \sim 10^{-7}$ or less), it is overwhelmed by the LO shot noise in the imaging experiment. In such a case, multiple images must be accumulated and spatial filtering must be performed to extract small signals. In the PM-SRS imaging of the LID and LOX, eight images were accumulated to increase the S/N by a factor of 2.8. In addition, we applied a Gaussian spatial low-pass filter to the image data. The corresponding point spread function in the *XZ* image was a 2D Gaussian function with a full width at half maximum (FWHM) of 4 μm, which was sufficient to analyze the microscopic surface structure of a skin tissue model. This spatial filtering further increased the S/N by a factor of 5.7.

4. Depth profile analysis

4.1. Detection of the reference depth boundary line

To obtain accurate depth profile data in hours-long skin penetration measurements, the depth position must be monitored because it can change during measurement due to sample drift or deformation. In addition, if the tissue surface is tilted and/or uneven in the field of view of the *XZ* image, simply averaging the SRS signal ΔI (X, Z) in the *X*-direction would provide a lower depth resolution. To avoid this error and perform analysis without losing depth resolution, we detected a reference boundary in the confocal image to align the relative depth position. Confocal reflection microscopy of the skin tissue provides a strong backscattered signal at the superficial SC layer [2]. Therefore, we determined the reference depth boundary from the uppermost signal peak position of the confocal reflection depth profile.

Figure S2 shows a confocal reflection image of the skin tissue model with a detected reference depth boundary. First, we applied a 2D Gaussian low-pass filter (FWHM: 4μm) to the *XZ* confocal image to reduce noise and perform accurate peak detection. Next, we detected the uppermost peak of the confocal reflection depth profile for each *X* position, using a common peak detection algorithm (‘findpeak’ function in MATLAB) in the *Z*-direction. The detected peak positions include some errors due to the roughness of the tissue surface, and the raw peak position plots on the *XZ* image plane show some points of discontinuity. Therefore, the plots were further smoothed by polynomial curve fitting (up to the third-order term) to determine the final reference boundary line. Thus, the relative depth-zero position ($Z_r = 0$) for each *Z* profile at *X* is defined as the *Z*-position at the boundary. Notably, the relative zero position is not exactly at the surface of the tissue, but at the middle of the SC layer, as discussed below.

Using the boundary line, the SRS depth image data were converted from the (X, Z) coordinates into the (X, Z_r) coordinate using shift arrays, and the data were then averaged in the *X*-direction to obtain the SRS depth profile. Finally, a 1D Gaussian smoothing filter was applied to the SRS profile to clearly visualize the differences between the depth profiles. The

corresponding response function of the spatial filtering along the *Z*-direction was a Gaussian function with a FWHM of 4.7 μm.

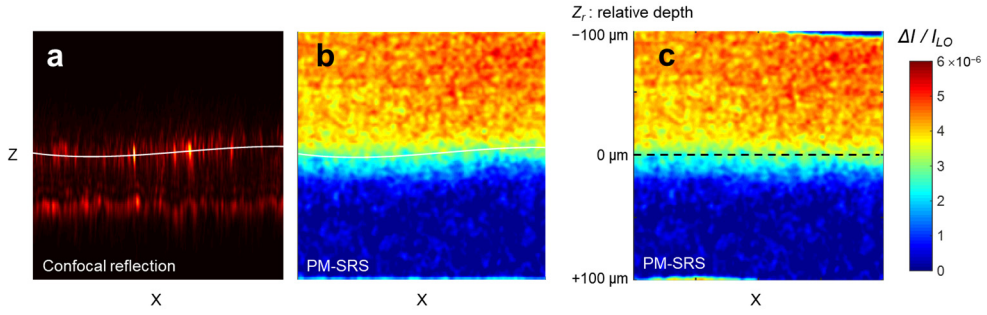

Fig. S2 (a) Detection of the reference depth boundary line (white line) from a confocal reflection image. (b) An PM-SRS image overlaid with the detected upper boundary. (c) The PM-SRS image converted to the XZ_r plane with the relative depth zero line (black dashed line).

4.2. Instrumental response function and relative focal depth

Calibration of the instrumental response function and the relative focal depth position of the confocal reflection and SRS microscopy are key requirements for accurate skin penetration analysis. Therefore, both depth profiles were measured using a linear stage scan in the *Z*-direction (Fig. S3) using an 8% LID solution sample, which was sandwiched between a glass slide and a coverslip. In the confocal reflection depth profile, a sharp signal peak with a FWHM of 5.5 μm was observed at the glass–liquid interface due to the large mismatch in the refractive index. The corresponding PM-SRS depth profile of the LID solution signal exhibited a smooth roll-off boundary. Here, we assumed a Lorentzian instrumental response function with a finite width. By fitting with a roll-off curve modeled by a convolution of the response function and a step function, the FWHM of the response function was determined to be 7 μm. This calibration measurement also verified that the foci of the two microscopes were located at the same depth position as the peak position of the confocal signal and the cutoff depth (at which the signal intensity reaches 50% of the maximum) of the SRS signal were both located at a depth of zero.

Next, we checked the depth resolution of the skin penetration test setup using a blank (0%) solution sample and an *in vitro* skin tissue model. We imaged a confocal reflection signal and the PM-SRS signal of a tissue signal at 1004 cm^{-1} (ring breathing mode of phenylalanine) and analyzed the depth profile to estimate the instrumental response function (Fig. S4). For the PM-SRS data, we calculated the deconvolution of the measured depth profile (using the 1D Richardson–Lucy algorism 'deconvlucy' in MATLAB) to obtain the instrumental response function and the deconvoluted depth profile. Again, we assumed a Lorentzian curve with a finite depth resolution as the PM-SRS response function and estimated the FWHM in the axial direction. This analysis showed that the depth resolution of the setup was estimated to be 10 μm. The reduced depth resolution can be explained by the spherical aberration of the skin penetration test setup (due to a 1-mm thick solution layer) and by the finite width of the skin tissue boundary (because the actual skin barrier is not an ideal step function). Although this is a limitation of the current setup, the depth resolution can be improved up to a few microns by installing a water-immersion objective with a high numerical aperture.

The blank test also revealed that the real surface position of the skin tissue model was located slightly at the negative relative depth ($Z_r \sim -6$ μm), rather than the relative depth zero ($Z_r = 0$) defined by the confocal peak position. A prominent tissue signal peak around the relative depth of zero suggests that the confocal reflection peak is located around the middle of the SC layer of the skin tissue model. Based on this result, the baseline skin penetration profile

shown in Fig. 4(a) was calculated from the convolution of a Lorentzian function with a finite width and a step function, which was centered at the real surface position estimated from the blank test (Z_r = −6 μm: vertical dashed line in Figs. 4(a) and 4(b)). Note that even though the deconvolution analysis is valid for depth profiles with a sufficient S/N, it does not provide a quantitative result for low-S/N data because of the noise amplification nature of the inverse filtering. Therefore, we did not apply the deconvolution method for skin penetration data analysis.

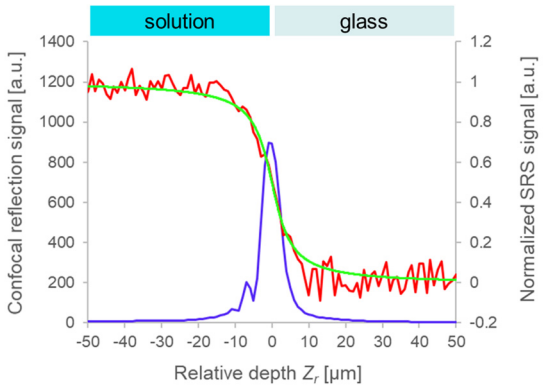

Fig. S3 Depth profiles of the confocal reflection microscopy (blue line) and the PM-SRS microscopy (red line). A zero depth was defined as the confocal peak position, i.e. the liquid–glass interface. An 8% LID solution sample was filled in the negative depth (Z_r < 0). The LID SRS signal was measured at 1092 cm^{-1} with a probe delay of 1.7 ps. A fitted depth profile modelled by convolution of a Lorentzian instrumental response function with a FWHM of 7 μm and a step function (green) is also shown.

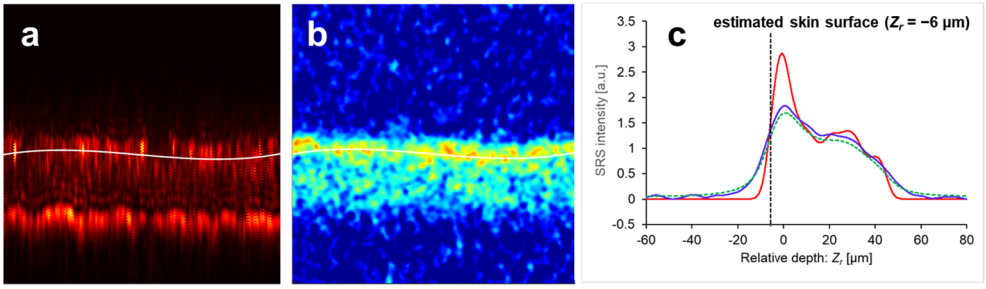

Fig. S4 Depth profiling of the tissue signal, (a) confocal reflection image and (b) PM-SRS image at 1004 cm^{-1} with a blank (0%) donor solution and an *in vitro* skin tissue model. (c) Depth profile deconvolution analysis: (blue line) the measured PM-SRS tissue signal profile at 1004 cm^{-1}, (red line) the reconstructed depth profile using the Richardson–Lucy algorithm ('deconvlucy' function in MATLAB with iterations = 20, damper = 0.1), where a Lorentzian instrumental response function with a depth resolution FWHM of 10 μm was assumed, (green dashed line) and the convolution of the reconstructed profile and the response function. The estimated skin surface is represented by a black dashed line.

4.3. Correcting scattering loss in SRS depth profiling

Another important calibration for quantitative depth profiling is the correction of the optical scattering loss [3]. In tissue imaging, because the total laser beam power reaching the focal point decays with the imaging depth owing to the scattering loss in the tissue, the depth profile of the signals should be corrected for the depth-dependent loss profile. To estimate the loss

factor, we measured the signal contrast of the PM heterodyne non-resonant background. By setting the relative probe delay to zero in the PM mode and setting the rotation angle of the detection polarizer to 45°, we obtained a strong heterodyne signal proportional to the real part of the third-order nonlinear susceptibility $Re\{\chi^{(3)}\}$ [1], which does not contain molecular-specific information. Here, the output intensities of the non-resonant and PM-SRS signals are proportional to $I_{pump}^{1.5}\, I_{PM}^{0.5}$ and $I_{pump}\, I_{PM}^{0.5}\, I_{LO}^{0.5}$, respectively; therefore, to the square of the total laser power, where I_{pump}, I_{PM}, and I_{LO} are the average intensities of the impulsive pump/Stokes pulse, PM probe, and LO probe pulses, respectively. Owing to the quadratic power scaling of both nonlinear contrast mechanisms, a depth-dependent loss profile derived from non-resonant signals can also be used to estimate the approximate loss profile of the PM-SRS signals.

A typical non-resonant background image and the corresponding depth profile are shown in Fig. S5. We estimated the depth-dependent signal loss profile from the image data, assuming that (i) the donor aqueous solution and the receiver solution have the same $Re\{\chi^{(3)}\}$, (ii) the depth-dependent loss profile is continuous, and (iii) the differential loss factors in the tissue layer and in the receiver solution layer are approximated by a single exponential decay function with different loss coefficients. The PM-SRS depth profiles of the drugs shown in Fig. 4 were corrected by dividing them by the estimated loss profile.

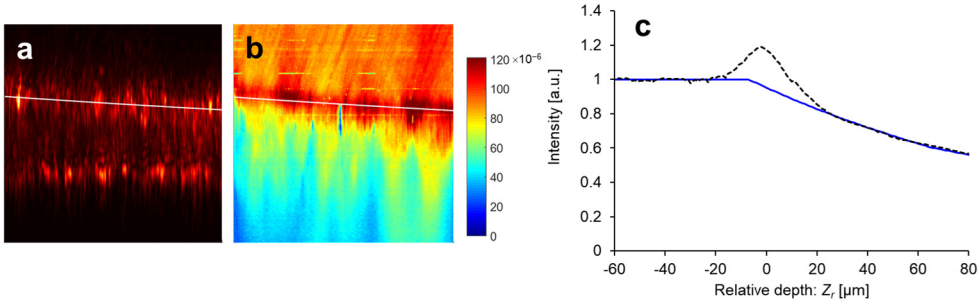

Fig. S5 Estimation of the depth-dependent signal loss profile: (a) confocal reflection image, (b) heterodyne-detected non-resonant background image (probe delay: 0 ps, PM mode), (c) depth profile of the measured non-resonant signal (black dashed line) and the estimated depth-dependent signal loss profile (blue solid line).

5. Optimizing the probe delay in PM-SRS imaging

The enhancement of the signal contrast by time-resolved detection relies on the difference between the vibrational lifetime of the target molecules and that of the tissue components. In principle, a higher signal-to-background ratio (S/B) can be achieved using a longer pulse delay time for signal detection. However, because the signal intensity per molecule (or sensitivity) generally decreases with the delay time, the probe delay should be set to the minimum value required to achieve the target S/B ratio. Figure S6 shows the probe delay dependence of the target drug Raman signals and the tissue background signals measured at the SC layer. In the experiment, we chose a delay time of 1.7 ps to obtain an S/B of more than 15 for all three test samples used. Note that this delay setting can be optimized for each individual drug Raman signal, as needed.

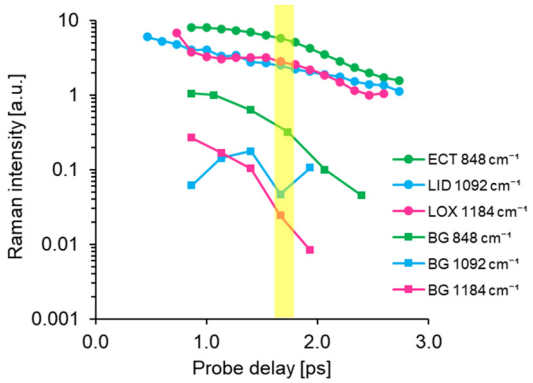

Fig. S6 Probe delay dependence of the target drug Raman signals and the tissue background signals. The Raman signals of donor solutions (ECT, LID and LOX: circles) and the corresponding tissue background signals at the target wavenumber (BG: squares) are plotted. The delay time used in the experiment (1.7 ps) is highlighted in a yellow band.

6. Spontaneous Raman spectroscopy

Prior to skin penetration experiments of the LID and LOX, we measured the spontaneous Raman spectra of the skin model and the test solution samples to identify the target molecular vibration modes (Fig. 3(a)). We used a home-built confocal Raman microscope with a 532-nm cw excitation laser (MSL-FN-532, CNI). The green laser beam was delivered to the confocal microscope through a polarization-maintaining single-mode fiber. The fiber output light was collimated, reflected by a dichroic mirror (RT532rdc, Chroma), and focused onto the sample with a water-immersion objective lens (CFI75 LWD 16XW, Nikon). Then, the backscattered light from the sample was collected by an identical objective lens. After the excitation laser light was blocked by an emission filter (RET537lp, Chroma), the collected light was delivered to a polychromator (MC-25V, Ritsu) equipped with an EM-CCD camera (C9100-14, Hamamatsu). The spectroscopy system covers the spectral range of 400 cm^{-1} – 1500 cm^{-1} with a spectral resolution of 10 cm^{-1}.

The spontaneous Raman spectrum of the skin tissue model was measured 10 μm below the tissue surface, and those of the drug samples were measured in 4% LID and 4% LOX aqueous solutions. The beam power used in the measurements at the sample was 14 mW, and the laser exposure time was 100 s. A typical S/B of the raw spontaneous Raman spectrum of the skin tissue model was ~0.05 for the 1004 cm^{-1} phenylalanine peak. The spectral baseline of all the data was subtracted to obtain the flat Raman spectra.

References

[1] T. Ito, Y. Obara, and K. Misawa, "Spectral focusing with asymmetric pulses for high-contrast pump–probe stimulated Raman scattering microscopy," APL Photon. **3**, 092405 (2018).
[2] P. Calzavara-Pinton, C. Longo, M. Venturini, R. Sala, and G. Pellacani, "Reflectance confocal microscopy for *in vivo* skin imaging," Photochem. Photobiol. **84**(6), 1421–1430 (2008).
[3] X. Chen, S. Grégoire, F. Formanek, J. B. Galey, and H. Rigneault, "Quantitative 3D molecular cutaneous absorption in human skin using label free nonlinear microscopy," J. Control. Release **200**, 78–86 (2015).